Published in final edited form as:
Nat Genet. 2009 March ; 41(3): 316–323. doi:10.1038/ng.337.

Bridging the gap between high-throughput genetic and transcriptional data reveals cellular pathways responding to alpha-synuclein toxicity

Esti Yeger-Lotem[1,3,*], **Laura Riva**[3,*], **Linhui Julie Su**[1,+], **Aaron D. Gitler**[1,6,+], **Anil Cashikar**[1,8], **Oliver D. King**[1,9], **Pavan K. Auluck**[1,4], **Melissa L. Geddie**[1], **Julie S. Valastyan**[1,5], **David R. Karger**[6], **Susan Lindquist**[1,2,#], and **Ernest Fraenkel**[3,6,#]

[1]Whitehead Institute for Biomedical Research, Cambridge, MA 02142 USA

[2]Howard Hughes Medical Institute, Cambridge, MA 02142 USA

[3]Department of Biological Engineering, Massachusetts Institute of Technology, Cambridge, MA 02139, USA

[4]Department of Pathology and Neurology, Massachusetts General Hospital, Boston, MA 02114 and Harvard Medical School, Boston MA 02115 USA

[5]Department of Biology, Massachusetts Institute of Technology, Cambridge, MA 02139, USA

[6]Computer Science and Artificial Intelligence Laboratory, Massachusetts Institute of Technology, Cambridge, MA 02139, USA

Abstract

Cells respond to stimuli by changes in various processes, including signaling pathways and gene expression. Efforts to identify components of these responses increasingly depend on mRNA profiling and genetic library screens, yet the functional roles of the genes identified by these assays often remain enigmatic. By comparing the results of these two assays across various cellular responses, we found that they are consistently distinct. Moreover, genetic screens tend to identify response regulators, while mRNA profiling frequently detects metabolic responses. We developed an integrative approach that bridges the gap between these data using known molecular interactions, thus highlighting major response pathways. We harnessed this approach to reveal cellular pathways related to alpha-synuclein, a small lipid-binding protein implicated in several neurodegenerative disorders including Parkinson disease. For this we screened an established yeast model for alpha-synuclein toxicity to identify genes that when overexpressed alter cellular survival. Application of our algorithm to these data and data from mRNA profiling provided functional explanations for many of these genes and revealed novel relations between alpha-synuclein toxicity and basic cellular pathways.

Cells live in a dynamic environment in which they confront various perturbations such as sudden environmental changes, toxins, and mutations. The response to such perturbations is

#To whom correspondence should be addressed. E-mail: lindquist_admin@wi.mit.edu (S. L.); fraenkel-admin@mit.edu (E.F.).
[7]Present Address: Department of Cell and Developmental Biology, The University of Pennsylvania, Philadelphia, PA, USA
[8]Present Address: Medical College of Georgia, Augusta, GA, USA
[9]Present Address: Boston Biomedical Research Institute, Watertown, MA, USA.
[*]These authors contributed equally to this work
[+]These authors contributed equally to this work

Summary: A novel approach that integrates genetic hits, differentially expressed genes and known molecular interactions reveals a dramatically enhanced view of cellular responses and was used to create the first cellular map of alpha-synuclein toxicity.

typically complex and comprises signaling and metabolic changes, as well as changes in gene expression. Revealing the cellular mechanisms responding to a specific perturbation may unravel its nature, thus illuminating disease mechanisms[1] or a drug's mode of action[2,3], and identify points of intervention with potential therapeutic value[4].

High-throughput experimental techniques including mRNA profiling and genetic screening are commonly used for revealing components of these response pathways because they provide a genome- and proteome-wide view of molecular changes. mRNA profiling experiments rapidly identify genes that are differentially expressed following stimuli. Genetic screening, including deletion, overexpression and RNAi library screens, identify genetic "hits", genes whose individual manipulation alters the phenotype of stimulated cells. However, each technique has obvious limitations for revealing the full nature of cellular responses. mRNA profiling experiments do not target the series of events that led to the differential expression. Genetic screens provide strong evidence that a gene is functionally related to the response process. Yet, this relationship is often indirect and hard to decipher, especially in high-throughput experiments that typically result in scores of relevant genes with various functions.

It has been noted previously in a few specific instances [2,5–9] that genetic screens do not identify the same genes as mRNA assays conducted in the same conditions. By analyzing the relationship between genetic hits and differentially expressed genes across 179 diverse conditions, we found that this discrepancy is, in fact, a general rule.

Furthermore, we found a striking bias in each technique that led us to a new, more coherent view of cellular responses. To bridge the gap between the two forms of high throughput analysis we developed an algorithm that exploits these experimental biases and that takes advantage of molecular interactions data. This approach simultaneously reveals (i) the functional context of genetic hits, and (ii) additional proteins that participate in the response yet were not detected by either the genetic or the mRNA profiling assays themselves.

Having validated our approach in a wide array of perturbations, we applied it to unravel cellular responses to increased expression of alpha-synuclein. Alpha-synuclein is a small human protein implicated in Parkinson disease whose native function and role in the etiology of the disease remain unclear [10]. We screened an established yeast model for alpha-synuclein toxicity [11,12] using an additional set of 3,500 overexpression yeast strains, exposing the multifaceted toxicity of alpha-synuclein. Application of our approach to the high-throughput genetic and transcriptional data of the yeast model illuminated response pathways whose manipulation altered cellular survival, and provided the first cellular map of the proteins and genes responding to alpha-synuclein expression.

The relationship between genetic hits and differentially expressed genes

In order to derive a comprehensive view of the relationship between genetic hits and differentially expressed genes identified in a particular condition, we analyzed published mRNA profiles and genetic hits for 179 distinct perturbations in yeast (Methods). These data included responses to a wide array of chemical and genetic insults affecting a multitude of cellular processes. For 30 of these perturbations complete genetic screens were reported, typically identifying >100 genetic hits; only partial genetic data are available for the remaining perturbations. The number of genetic hits, differentially expressed genes and genes common to both for each perturbation are given in Table 1 and Supplementary Table 1. Intriguingly, in almost all cases the overlap was astonishingly small and statistically insignificant ($p>0.05$, Methods).

One possible explanation for the poor overlap between genetic hits and differentially expressed genes is that each assay may be biased toward distinct aspects of cellular responses. Analysis

of Gene Ontology (GO) enrichment confirmed this hypothesis (Methods). The combined hits from all 179 genetic screens were highly enriched for the annotations biological regulation (23.3%, $p<10^{-82}$), transcription (14%, $p<10^{-44}$) and signal transduction (6.3%, $p<10^{-30}$). In contrast, the regulated genes from all perturbations were enriched mostly for various metabolic processes (e.g., organic acid metabolic process 7.1%, $p<10^{-18}$) and oxidoreductase activities 7.2%, $p< 10^{-34}$). To ensure these patterns of enrichment do not stem from a handful of data sources but reflect a general tendency, we also analyzed the 30 perturbations for which complete data were available. We found the same enrichment trends, regardless of whether these perturbations were analyzed individually (Supplementary Table 2) or whether all 30 datasets were combined (Supplementary Table 3). Complete enrichment analyses appear in Supplementary Text. Thus, we find that genetic assays tend to probe the *regulation* of cellular responses, while mRNA profiling assays tend to probe the *metabolic aspects* of cellular responses.

The striking differences in annotations between genetic hits and differentially expressed genes imply that each gene set alone often provides a limited and biased view of cellular responses. In fact, this hypothesis was often borne out in cases where the pathways are well-studied by other, more classical methods of genetic and molecular biological research. In the yeast DNA damage response pathway, for example, a genetic screen [4] detected proteins that sense DNA damage (Mec3, Ddc1, Rad17 and Rad24), while mRNA profiling detected repair enzymes such as Rnr4 [13]. Yet core components of this pathway that had been uncovered by other intense investigations over many years, such as the signal transducers Mec1 and Rad53 and the transcription factor Rfx1, remained undetected by either high-throughput assay.

If we are to fully reap the benefits of applying high-throughput methods to new problems and under-explored biological processes, it is essential that we find new routes to connect these data and obtain a true picture of the regulation of cellular responses. Here we provide a novel framework that bridges the gap between genetic and transcriptional data. Based on known pathways such as the response to DNA damage discussed above, we expect that some of the genetic hits, which are enriched for response regulators, will be connected via regulatory pathways to the differentially regulated genes, which are the output of such pathways. Discovering these pathways may uncover additional components of the cellular response to perturbation that are missing from the experimental data (Figure 1).

ResponseNet algorithm for identification of response networks

The ResponseNet algorithm identifies molecular interaction paths connecting genetic hits and differentially expressed genes that may include hidden components of the cellular response (Figure 1). The yeast *Saccharomyces cerevisiae* provides a powerful model system for such analysis due to the extensive molecular interactions data now available (Methods and Supplementary Table 4). Taking advantage of these resources we assembled an integrated network model of the yeast interactome that contains protein-protein interactions, metabolic relations and protein-DNA interactions detected by various methods with different levels of reliability[14]. The resulting interactome relates 5,622 interacting proteins and 5,510 regulated genes, which are represented by network nodes, via 57,955 molecular interactions, which are represented by network edges.

Our representation of the interactome has two important features that facilitate identification of pathways relating genetic hits to transcriptional changes. First, we chose to highlight the role of transcriptional regulatory proteins in determining expression changes by representing differentially expressed genes and their protein products as separate nodes. The only protein nodes that are connected to gene nodes are transcriptional regulatory proteins, and the edges between protein and gene nodes represent observed protein-DNA interactions. Edges between

two protein nodes represent protein-protein interaction data. Thus, all pathways connecting genetic hits to the differentially expressed genes must pass through a transcriptional regulatory protein (Supplementary Figure 1). Second, because interactions vary in their reliability, each edge was given a weight that represents the probability that the connected nodes interact in a response pathway. The probabilities were computed using a Bayesian method that considers the types of experimental data supporting the putative interaction and that favors interactions among proteins acting in a common cellular response pathway (Methods).

Due to the vast number of edges, a search for all interaction paths connecting the genetic hits to the differentially expressed genes typically results in "hairball" networks that are very hard to interpret (Figure 2A). One approach to this problem is to identify the highest probability paths. However, pioneering approaches that searched an interactome for high-probability paths had to limit the output path lengths to 3 edges for computational complexity issues[15,16]. We aimed for a solution that would (i) pick the subset of genetic hits most likely to modulate the differentially expressed genes without limiting it *a priori* to known regulatory genes, (ii) identify and rank intermediary proteins that are likely to be part of response pathways but escaped detection by high-throughput methods, and (iii) connect the proteins via a high-probability interactome sub-network without restricting its topology.

We reasoned that these requirements could elegantly be met using a "flow algorithm", a computational method that has been employed previously to analyze signaling or metabolic networks that have already known topology (e.g.,[17]). In these algorithms flow goes from a source node to a sink node through the graph edges; edges can be associated with a capacity that limits the flow and are also associated with a cost. (As a loose analogy, this resembles water finding the path of least resistance through a complex landscape.) Because we sought to discover the topology of the unknown response pathways connecting genetic hits and differentially expressed genes we required that flow pass from genetic hits through interactome edges to transcriptional regulators of the regulated genes (Supplementary Figure 1). We then formulated our goal as a minimumcost flow optimization problem [18]: Cost was defined as the negative log of the probability of an edge. Hence, by minimizing the cost the algorithm gives preference to high-probability paths (Methods).

The solution to the optimization problem is a relatively sparse network that connects many of the genetic hits to many of the regulated genes through known interactions and intermediary proteins (Figure 2B). These intermediary proteins were not identified by either high-throughput genetic analysis or mRNA profiling, but are predicted by the algorithm to play a part in the response. The proteins in the solution are ranked by the amount of flow they carry. The more flow that passes through a protein, the more important it is in connecting the genetic and transcriptional datasets.

Validation of the ResponseNet algorithm

To determine if ResponseNet provides valid biological insights, we used it to connect genetic and transcriptional data from perturbations in well-studied pathways. We then asked if ResponseNet revealed the proteins and pathways that are missing from the genetic and transcriptional data, but that had previously been gleaned from individual analyses. For example, we used ResponseNet to analyze genetic hits[19] and transcriptional[20] data collected from a strain deleted for the gene encoding Ste5, a scaffold protein that coordinates the MAP kinase cascade activated by pheromone (Figure 2B). The nodes selected by ResponseNet were highly enriched for proteins functioning in the pheromone response pathway (46%, $p<10^{-18}$), thus revealing the perturbed biological process. The highly ranked intermediary proteins provided biologically meaningful connections between the data sets, as they included key regulators of the pheromone response as well as Ste5, the source of perturbation.

The algorithm also performed well in analyzing the much more complex cellular response to DNA damage[4,21,22]. The nodes discovered by ResponseNet were highly enriched for the GO categories response to DNA damage stimulus (21%, $p<10^{-14}$) and DNA repair (19%, $p<10^{-14}$). Indeed, the most highly ranked part of the network contained core members of the pathway that had previously been uncovered by years of intense investigation but were not detected by high-throughput screens, including the signal transducers Mec1 and Rad53, members of the RFC complex (Rfc2-Rfc5) and the transcription factor Rfx1 (Figure 2C).

To test ResponseNet more broadly, we evaluated its ability to identify hidden components in the cellular response to over one hundred distinct perturbations corresponding to inactivations of well-annotated genes (Methods). For each such perturbation the genetic hits set consisted of the genetic interactors of the inactivated gene (e.g., synthetic lethals), and the differentially expressed genes were based on mRNA profiling of the inactivated strain [20]. The identity of the inactivated gene was hidden from the algorithm, and was used to evaluate the predicted network. ResponseNet output was considered successful in revealing the cellular response to the perturbation if the hidden nodes it identified fulfilled one of two criteria: (i) they included the inactivated gene that was the source of perturbation, or (ii) they were significantly enriched for a specific biological process attributed to the inactivated gene. Significance was determined relative to networks generated using randomization techniques (Methods and supplementary text).

ResponseNet success rates are given in Table 2 and Supplementary Table 5. In total, ResponseNet predictions were successful in 63% of the cases. This rate of success is relatively high considering that for the majority of the cases (85%) genetic hits data were rather limited (a median of 14 genetic hits) and no high-throughput genetic screening data are yet available. Notably, ResponseNet typically selected only 1% of the yeast proteins as relevant for the response. Despite the fact that relevant interactions might be missing from our data or have low probability compared with alternative paths, in a third of the cases the inactivated gene was highly ranked among this small fraction.

A map of cellular pathways responding to alpha-synuclein toxicity

Having established the validity of our method to uncover connections between otherwise disparate high-throughput datasets, we applied ResponseNet to investigate the cellular toxicity associated with alpha-synuclein (α-syn). α-syn is a small lipid-binding protein that is natively unfolded when not bound to lipids and prone to forming toxic oligomers [23]. It that has been implicated in several neurodegenerative disorders, most particularly Parkinson disease (PD). α-syn is the main component of Lewy bodies, cytoplasmic proteinaceous inclusions that are a hallmark of PD [24]; locus duplication or triplication of α-syn lead to familial forms of PD [25, 26], and increased expression of α-syn leads to neurodegeneration in several animal models [27]. α-syn is linked to alterations in vesicle trafficking [12,28] and mitochondrial function [29], yet despite immense efforts, the cellular pathways by which α-syn leads to cell death are just beginning to be uncovered.

The yeast *S. cerevisiae* provides a powerful system for studying the molecular basis of α-syn toxicity that result from its intrinsic physical properties. Expression of human α-syn in yeast yields several dosage-dependent defects that are also found in mammalian systems, such as lipid droplet accumulation in the cytosol, the production of reactive oxygen species and impairment of the ubiquitin-proteasome system [11]. An initial overexpression screen in yeast for genes that modify α-syn toxicity tested 2,000 strains and identified a class of genes functioning in ER to Golgi vesicle trafficking, leading to the observation that α-syn causes an ER to Golgi vesicle trafficking block. One of these genes, Ypt1/Rab1, a GTPase protein, was

tested in neuronal models of PD and was found to rescue dopaminergic neurons from α-syn toxicity [12].

We now report other results from that screen and the results of screening an additional set of 3,500 overexpression yeast strains, thereby covering in total 85% of the yeast proteome. We identified a diverse group of genes including 54 suppressors and 23 enhancers of α-syn toxicity, many with clear human orthologs (Table 3). Major classes of genes that emerged include vesicle-trafficking genes, kinases and phosphatases, ubiquitin-related proteins, transcriptional regulators, manganese transporters, and trehalose biosynthesis genes. Significantly enriched GO categories included ER to Golgi vesicle-mediated transport (12%, $p=6.2*10^{-5}$), phosphatases (9.1%, p=0.0028) and transcription factors (6.5%, p=0.047). While the identification of additional vesicle trafficking and ubiquitin-related genes is consistent with the defects caused by α-syn expression in yeast, the identification of trehalose biosynthesis genes and manganese transporters was new and intriguing. Trehalose was recently shown to promote the clearance of misfolded mutant α-syn [30], and manganese exposure has been linked with Parkinson-like symptoms albeit with a distinct underlying pathology[31]. Notably, another suppressor we identified is homologous to the human PD gene PARK9.

Park9 and the human homologs of seven other genetic modifiers from diverse functional classes (Hrd1, Ubp3, Pde2, Cdc5, Yck3, Sit4 and Pmr1) were found to be efficacious in neuronal models, validating the yeast model as meaningful to α-syn toxicity in neurons (Gitler et al.; manuscript submitted). The genes identified by the screen therefore begin to unravel the surprisingly multifaceted toxicity of α-syn. Importantly, they provide novel causal relations between α-syn expression and toxicities previously associated with PD but not specifically linked to α-syn. A detailed description of the various gene classes and their potential relation to PD appears in the Supplementary Text.

The transcriptional profile occurring in response to α-syn toxicity was determined in a separate study (Supplementary Text; Su et al.; manuscript submitted). Up-regulated genes prominently included genes with oxidoreductase activities (13%, $p<10^{-9}$). Down-regulated genes included ribosomal genes (28%, $p<10^{-30}$), as commonly observed under stress [32]. More specific to α-syn toxicity, the down-regulated genes were strikingly enriched for genes encoding proteins localized to the mitochondria (60%, $p<10^{-44}$) and for genes involved in generation of precursor metabolites and energy (18%, $p<10^{-15}$).

The genetic and transcriptional data obtained in this model system exemplify both the power and the limitations of the current approaches. These technologies reveal the wide range of cellular functions that are altered by α-syn expression. Yet the precise roles of the genetic hits and differentially expressed genes in the cellular response are unclear. For example, we checked whether the ubiquitin-related proteins that emerged from the genetic screen affect α-syn degradation. However, in strains overexpressing these ubiquitin-related genes we did not detect changes by flow cytometry in steady-state α-syn protein levels (Supplementary Figure 2). As with our previous analyses (above), the overlap between the data obtained from the genome-wide genetic screen and mRNA profiling assay was minor and statistically insignificant (four genes, p=0.96).

Applying ResponseNet to these disparate datasets revealed a more coherent view of the cellular response (Supplementary Figure 3). The resulting network provided context to a large portion of the data: 34 (44%) genetic hits and 166 (27%) differentially expressed genes were linked to each other through 106 intermediate connections. These include two thirds of the protein kinase, phosphatase and ubiquitin-related genetic hits, illuminating their intricate role in the response to α-syn. For example, ResponseNet suggests that the genetic suppressor Rck1, a kinase known to respond to oxidative stress, functions through its interactions with the Cad1

transcription factor, and that this sub-network explains the differential transcriptional of seven genes (Supplementary Figure 3J). Similarly, ResponseNet identifies a set of transcriptional changes that it traces back to the genetic hits Bre5 and Ubp3, which form a deubiquitination complex (Supplementary Figure 3C).

The major cellular pathways responding to α-syn toxicity included ubiquitin-dependent protein degradation, cell cycle regulation and vesicle trafficking pathways, all of which have previously been associated with PD (Supplementary text and Supplementary Figure 3). Impairment of the ubiquitin proteasome system[33] and mutations in ubiquitin-related genes (parkin and uch-L1) underlie sporadic and familial forms of PD. Interestingly, parkin is associated with the SCF ubiquitin ligase complex [34], components of which were selected by ResponseNet. Inappropriate cell cycle regulation has also been implicated in neuronal cell death in PD [35,36], and ResponseNet predicted several regulators of mitosis and early meiosis. Below we focus on additional ResponseNet predictions that relate to known aspects of PD including nitrosylation, mitochondrial dysfunction and the heat shock response.

Nitrosative stress

Fzf1 was the only gene identified in the screen related to nitrosative stress [37]. However, ResponseNet connected it to four up-regulated transcripts, including Pdi1, a protein disulfide isomerase (PDI) (Figure 3A). Intriguingly, the up-regulation of human PDI protects neuronal cells from neurotoxicity associated with ER stress and protein misfolding (both of which are linked to α-syn expression), and, further, PDI has been found to be S-nitrosylated in PD [38]. We found that increased expression of α-syn causes increased S-nitrosylation of proteins (Figure 3B). This result is surprising as nitrosative responses in yeast cells were long thought to represent a defense mechanism against other microbes. Very recently it was shown that yeast synthesize NO in response to exogenous H_2O_2 39, suggesting that the nitrosylation of specific proteins is a highly conserved response to oxidative stress.

Mitochondrial dysfunction

Mitochondrial dysfunction and oxidative stress have been strongly linked with PD [40], and were recently associated specifically with α-syn (e.g., [41]). Although mitochondrial dysfunction was a prominent signature in the microarray data (Su et al.; manuscript submitted), the genetic hits contained only a few genes clearly related to mitochondria. ResponseNet identified two connected components related to mitochondrial dysfunction. One component contained the suppressor Hap4, a transcriptional activator of respiratory genes, directly connected to several of the differentially expressed genes (Supplementary Figure 3B). The other component contained regulators of the retrograde signaling pathway, which senses mitochondrial dysfunction (Mks1, Rtg2 and Grr1 [42], Supplementary Figure 3E).

Heat shock

The induction of heat shock response directly or via chemical inhibition of Hsp90 [43] suppresses α-syn toxicity in many model systems including yeast, flies, mice and human cells (e.g., [44, 45]). However, heat shock related genes were conspicuously absent among the list of genetic suppressors. Nonetheless, ResponseNet predicted the involvement of two highly conserved heat shock regulators, the chaperone Hsp90 (isoform Hsp82, Supplementary Figure 3A) and the heat shock transcription factor Hsf1 (Figure 4A). Interestingly, ResponseNet predicted that the toxicity suppressor Gip2, a putative regulatory subunit of the Glc7 phosphatase, interacts with Gac1. Gac1 is a regulatory subunit of the Glc7 complex, which is known to activate Hsf1[46]. This connection suggested that Gip2 overexpression might induce a heat shock response and prompted us to test it. Indeed, we found that strains overexpressing Gip2 show elevated levels of heat shock proteins (Figure 4B). ResponseNet therefore provided a

mechanistic explanation for the suppression of α-syn toxicity achieved by Gip2 overexpression and identified a new player in the regulation of the ancient heat shock response.

We also identified cellular pathways whose relation to α-syn toxicity was initially obscure, raising the possibility that they may be interesting avenues for future research. Below we focus on two such highly-conserved pathways, the mevalonate/ergosterol pathway that is targeted by the cholesterol lowering statin drugs, and the target of rapamycin (TOR) pathway.

The mevalonate/ergosterol biosynthesis pathway not only synthesizes sterols, but also synthesizes other products with connections to α-syn toxicity such as farnesyl groups required for vesicle trafficking proteins and ubiquinone required for mitochondrial respiration. ResponseNet ranked highly Hrd1, which regulates the protein target of statins, and the predicted intermediary Hap1, a proposed transcriptional regulator of the pathway [47] (Supplementary Figure 3A). In addition, the α-syn mRNA profile was modestly correlated with the profile of yeast treated with lovastatin ($r=0.32$, $p< 10^{-93}$, Su et al; manuscript submitted), and several genetic hits could be also associated with products of the pathway (dependent enzymes Bet4 and Cax4, farnesylated proteins Ypt1 and Ykt6 and putative sterol carriers Sut2, Osh2, and Osh3). We therefore tested the effect of lovastatin, which selectively inhibits the highly conserved HMG-CoA reductase of yeast as well as that of mammalian cells, on α-syn toxicity. Addition of 5μM lovastatin to the media caused a further reduction in growth to strains overexpressing α-syn (Figure 5A), but did not reduce growth of either wild-type controls or of cells expressing another toxic protein, a glutamine-expansion variant of huntingtin exon I [48] (Supplementary Figure 4). We further tested ubiquinone, a downstream output of this pathway, reasoning that its down-regulation through the action of α-syn might increase cellular vulnerability. Indeed, the addition of ubiquinone-2 to the media provided a modest suppression against α-syn toxicity. Ubiquinone is an antioxidant, but this was not a non-specific antioxidant response as the antioxidant N-acetylcysteine had no effect (Supplementary Figure 5).

The TOR pathway has been related to other neurodegenerative diseases [49,50]. ResponseNet identified the TOR pathway proteins Tor1, Tor2 and their target transcription factors as intermediary between the genetic hit Lst8 and several up-regulated genes involved in spore wall formation (a vectorially directed secretory process in yeast) and vacuolar protein degradation (Figure 5B). We found that addition of the TOR-inhibitor rapamycin to the media markedly enhanced the toxicity of α-syn. Indeed, a low dose α-syn, which is otherwise innocuous, became toxic (Figure 5C). Establishing the specificity of this effect to α-syn, rapamycin did not reduce growth of cells expressing glutamine expansion variants of huntingtin exon I (Supplementary Figure 6).

Discussion

We provide a novel framework in which genetic, physical and transcriptional data naturally complement each other in the context of cellular response to biological perturbations. Although the complementary nature of these data has been noted [2,5–9,51–55], a systematic analysis of the relationship between stimulus-specific genetic modifiers and transcriptional responses has been lacking. Here we find that in response to over 150 distinct stimuli differentially expressed genes and genetic hits are consistently disparate (Table 1).

Our analysis suggests some interesting possible explanations for the discrepancy between these two types of experiments. We have observed that differentially transcribed genes are disproportionately involved in metabolic processes. These genes are less likely to appear as genetic hits because metabolic processes tend to be robust against single mutations [56]. We have also found that genetic hits are biased towards regulatory proteins. Since deletion or over-expression of a regulatory protein is likely to dramatically alter cellular signaling, this bias is,

in hindsight, quite reasonable. However, why are regulatory proteins rarely found to be differentially transcribed?

The lack of an observed transcriptional response by regulatory proteins could arise from either technical or biological reasons. From a technical perspective, regulatory proteins are commonly controlled post-transcriptionally, and therefore show no change in mRNA levels. For example, purely post-transcriptional changes in HSF1 activity can produce enormous changes in the expression of protein chaperones. Further, since many of these proteins have very low transcript concentrations[57], alterations in their mRNA levels may be below the detection limits of microarray platforms.

Several possible biological explanations for the dearth of regulatory proteins among the differentially transcribed genes would add to this effect. Proteins that initiate a signaling response such as the components of the "sliding clamp checkpoint," which detects DNA damage, must be present at all times in order to detect environmental changes. In addition, proteins that transmit signaling information but that do not initiate a response (such as kinases) may also need to be kept at relatively constant levels, as changes in the levels of these proteins can dramatically alter the systems-level properties of a signaling pathway, resulting in surprising biological effects[58]. In such cases, it is precisely because changes in the expression level of a genetic hit produces such a readily detectable phenotype that the expression of the gene is maintained at a constant level.

The discordance between genetic hits and differentially expressed genes has implications for the search for therapeutic strategies. In yeast, inactivating a differentially expressed gene is no more likely to affect cell viability than targeting a randomly chosen gene. Yet bridging the gap between these data can potentially reveal additional intervention points that may be targeted by drugs.

Deciphering the role of genetic hits identified under conditions such as stress or disease is a complex task. Our analysis indicates that this task can be facilitated by incorporating molecular interactions data. Previous interactions-based interpretations often focused on graph-related properties of the data, such as neighboring genes representing functionally related proteins[59, 60], connected components representing functional modules [61] and network hubs representing key proteins [62]. However, these approaches have limited power to reveal mechanistic insights especially when the underlying networks become dense.

We provide a novel scheme to interpret the functional role of genetic hits. By focusing on their regulatory relationship with differentially expressed genes and using the interactome as the underlying architecture, our approach represents an important step toward fully mechanistic models for the regulation of cellular responses. As described for the deletion of Ste5 and the response to DNA damage, ResponseNet can provide a richer framework for previously explored pathways (Figure 2). More importantly, ResponseNet has the power to uncover connections between high-throughput data sets that reveal underlying biological processes in cases for which little is known, as was true for α-syn. The resulting networks provide extended views of cellular responses as they incorporate relevant proteins not discovered in the high-throughput assays themselves (Figure 2).

Our computational approach is based on a flow algorithm to connect the genetic hits and differentially expressed genes. Unlike intriguing studies that link a target gene with its causal transcriptional change[13,15,16,63–66], a flow-based approach allows for a global, efficient and simultaneous solution for multiple target genes that puts no *a priori* bounds on the structure of the output. In fact, the predicted output networks have rich structures with half of all paths of length of 3 or more. The ability of ResponseNet to analyze interactome data containing tens

of thousands of nodes and edges make it well-suited to analyzing the accumulating data from other species or other techniques[67].

We applied our approach to a yeast model for α-syn pathobiology implicated in PD. The complexity of PD and the multifaceted nature of the toxicities associated with just one protein, α-syn, mandate their investigation via systems biology approaches. We identified 77 genes whose overexpression altered α-syn toxicity (Table 3). In addition to genes involved in vesicle trafficking (as previously reported), these included genes involved in protein degradation, cell cycle regulation, nitrosative stress, osmolyte biosynthesis and manganese transport. This screen established an interface between α-syn and a large number of cellular and environmental factors previously linked to neuropathology and, in some cases, specifically to Parkinsonism, but not specifically linked to α-syn. Many of the genes we identified are highly conserved in humans, where they may exert similar affects. Indeed, eight out of nine toxicity modifiers we have now tested had similar effects on α-syn toxicity in yeast and in neuronal systems (Gitler et al; manuscript submitted).

Application of ResponseNet to the disparate high-throughput genetic and transcriptional data of the α-syn model succeeded in providing a functional context to many of the genetic hits identified in our yeast screen (Supplementary Figure 3). It uncovered the involvement of the heat shock response, the TOR pathway and the mevalonate/ergosterol pathway in the response to α-syn expression, which we experimentally validated (Figure 3–Figure 5). Of these, the mevalonate/ergosterol pathway is of special interest as its perturbation could potentially alter a variety of downstream pathways, including protein farnesylation and ubiquinone biosynthesis that are closely related to the vesicle trafficking defects and mitochondrial dysfunction observed in the yeast model. The fact that several of the yeast modifiers of α-syn toxicity act similarly in neuronal systems suggests that the pathways we identified in yeast are relevant in neuronal systems. Indeed, a link between sterol biosynthesis and the etiology of PD surfaced recently in man. PD patients have significantly lower levels of low-density lipoprotein (LDL) cholesterol than their spouses [68], and low levels of LDL preceded the appearance of PD in a group of men of Japanese ancestry [69].

The global picture we obtained by integrating high-throughput genetic, transcriptional and physical yeast data demonstrates the power of integrative approaches to illuminate under-explored cellular processes. As high-throughput assays are becoming routine in the study of complex disease and developmental processes, approaches for deciphering these data based on their underlying characteristics are vital.

Materials and Methods

Genetic and transcriptional datasets

Datasets for chemical perturbations were downloaded from original papers. Genetic hits for gene inactivation were defined as the set of proteins found to genetically interact with the inactivated gene. These data were downloaded from SGD [19] and included all types of genetic interactions. Transcriptional data consisting of differentially expressed genes showing at least a two-fold change in expression with a p-value ≤ 0.05 were extracted from [20], or else were defined according to original papers. Chemical perturbation assays were paired if the concentrations of the chemical were comparable in both assays.

Interactome data description

The interactome is represented as a graph $G = (V,E)$ that consists of nodes (vertices) V representing genes and proteins, and a set of bidirectional and directed edges E representing their interactions. Different nodes in the network represent a gene and its corresponding protein.

Bidirectional edges between protein nodes in the interactome consisted of:

- **i.** Physical protein-protein interactions, which were downloaded from [70] and from BioGRID release 2.0.30.
- **ii.** Interactions between two proteins if they both appeared in the same literature-curated protein complex, downloaded from MIPS [71].
- **iii.** Metabolic interactions between two enzymes, if the substrate of one was the product of the other, based on the metabolic map of *S. cerevisiae* 17.

Directed edges in the interactome consisted of:

- **i.** Edges from a protein node to a gene node if there was evidence from either literature or ChIP-chip assays [72–74] that the protein was a probable transcriptional regulator of the gene.
- **ii.** Edges from one protein node to another if both proteins acted as transcriptional regulators and the first regulated the second.

Supplementary Table 4 lists the number of interacting pairs per interaction type in the interactome.

Weighting scheme for interactome edges

Each edge $(i,j) \in E$ between node i and node j of the interactome is characterized by a weight w_{ij} calculated as follows:

Interactions between protein nodes—We developed a Bayesian weighting scheme that favors interactions between proteins functioning within a common response pathway (*RP*). Each interacting protein pair p_i,p_j was associated with an interaction vector Ip_i,pj, where vector entry $I_k\ p_i,p_j$ serves as an indicator function for interaction evidence of type k. For example, I *"two-hybrid HTP"* p_i,p_j was set to 1 if p_i interacted with p_j in a high-throughput two-hybrid experiment. Each interacting protein pair p_i,p_j was assigned a weight w_{ij} reflecting the probability that p_i,p_j function in a randomly selected response pathway (denoted $RP_{\mathrm{pi,pj}}=1$) based on their interaction evidence vector $I_{pi,pj}$. By Bayes' rule,

$$w_{\mathrm{ij}}=\mathrm{p}(\mathrm{RP}_{p_ip_j}=1\,|\,I_{p_ip_j})=\mathrm{P}(I_{p_ip_j}|\,\mathrm{RP}_{p_ip_j}=1)\mathrm{P}(\mathrm{RP}_{p_ip_j}=1)/\mathrm{P}(I_{p_ip_j})\text{ , where}$$
$$\mathrm{P}(I_{p_ip_j})=\mathrm{P}(I_{p_ip_j}\,|\mathrm{RP}_{p_ip_j}=1)\mathrm{P}(\mathrm{RP}_{p_ip_j}=1)+\mathrm{P}(I_{p_ip_j}|\,\mathrm{RP}_{p_ip_j}=0)\mathrm{P}(\mathrm{RP}_{p_ip_j}=0).$$

We assumed that different types of evidence are conditionally independent, so that $\mathrm{P}(I_{p_ip_j}|\mathrm{Rp}_{p_ip_j})=\prod_k \mathrm{P}(I_{kp_ip_j}|\mathrm{RP}_{p_ip_j})$. To estimate the prior probability P(*RP*) and the conditional probability table associated with each evidence type $\mathrm{P}(I_k|\ RP)$ we compiled the following:

1. A set of response pathways containing 54 response-specific processes according to GO process annotations (e.g., response to osmotic stress GO:0006970).
2. A set of positive examples containing all interacting protein pairs functioning in a common response pathway (see 1 above) based on reliable GO process annotations. To exclude less reliable sources of annotation we used only GO evidence relying on direct assay or expert knowledge (GO evidence codes IC, IDA and TAS).
3. A set of negative examples composed of interacting protein pairs known not be in a common response pathway similar to [75].

Supplementary Table 6 lists the resulting weights associated with individual evidence types.

Some edge weights w_{ij} were close to 1, which was unrealistic biologically and could instead indicate unusually well-studied proteins [76] or imperfectness of the assumption of conditional independence. To prevent such edges from dominating the predicting response networks, and to place all edges with high enough weights on equal footing, the weights w_{ij} were capped to a maximum value of 0.7. Notably, small changes in this value (0.7±0.1) gave similar results in the subsequent analyses.

Interactions between protein and gene nodes—These weights were designed to reflect the interaction's reliability based on experimental evidence and conservation. "ChIP-chip interactions" refer to interactions discovered by the ChIP-chip method. "ChIP-chip motif interactions" refer to those ChIP-chip interactions for which the gene's upstream sequence contained the binding motif of the specific transcription factor. "Reliable interactions" included those ChIP-chip motif interactions for which the motif occurrence in the gene's upstream sequence was conserved in at least two other *Saccharomyces sensu stricto* species, as well as literature-curated interactions. The weight of reliable interactions was set to 0.7. The weight of remaining "ChIP-chip interactions" was set to the fraction of "ChIP-chip interactions" that were also reliable (0.51), and similarly the weight of remaining "ChIP-chip motif interactions" was set to the fraction of "ChIP-chip motif interactions" that were also reliable (0.59).

Linear programming formulation

The inputs to ResponseNet consist of the weighted interactome $G = (V,E)$, the genetic hits data set $Gen \subset V$ and the transcriptional data set $Tra \subset V$ identified following a specific perturbation. Each edge $(i,j) \in E$ is characterized by a weight w_{ij} representing its probability (as described above), and by a capacity $c_{ij} = 1$.

For each perturbation the graph G is updated as follows:

1. $V' = V \cup \{S,T\}$, where S and T are auxiliary nodes representing the source and sink, respectively.
2. $E' = E \cup (S,i)_{\forall i \in \mathrm{Gen}} \cup (i,T)_{\forall i \in Tra}$, thus connecting S to the genetic hits and T to the differentially expressed genes data using directed edges.
3. $c_{Si} = \frac{|\mathrm{strength}_i|}{\sum_{j \in \mathrm{Gen}} |\mathrm{strength}_j|}, \forall i \in \mathrm{Gen}$. The strength of each genetic hit is measured by the variation it confers on the number of colonies per drop, if available, otherwise strengths are taken to be uniform. Thus the capacities associated with the edges between the source S and the genetic hits are proportional to the strength of each genetic hit, and can be viewed as a prior for including the gene in the output.
4. $c_{iT} \frac{|\log_2(\mathrm{strength}_i)|}{\sum_{j \in \mathrm{Tra}} |\log_2(\mathrm{strength}_j)|}, \forall i \in \mathrm{Tra}$. The strength is measured by either the fold-change in its transcript level or the p-value associated with it, depending on their availability. Thus the capacities associated to the edges between each transcriptional hit and the sink T are proportional to the logarithm of the gene strength, and can be viewed as a prior for including the gene in the output.
5. $w_{Si} = c_{Si}\ \forall i \in Gen$ and $w_{iT} = c_{iT}\ \forall i \in Tra$.

Let f_{ij} denote the flow from node i to node j, and let $F = \{f_{ij}\}$ denote the solution to the following optimization problem: min

$$\min\left(\left(\sum_{i\in V',j\in V'} -\log(w_{ij})^{*} f_{ij}\right) - \left(\gamma^{*}\sum_{i\in \mathrm{Gen}} f_{Si}\right)\right) \quad \gamma \geq 0 \tag{1}$$

subject to:

$$\sum_{j\in V'} f_{ij} - \sum_{j\in V'} f_{ij} = 0 \quad \forall i \in V' - \{S, T\} \tag{2}$$

$$\sum_{i\in \mathrm{Gen}} f_{Si} - \sum_{i\in \mathrm{Tra}} f_{iT} = 0 \tag{3}$$

$$0 \leq f_{ij} \leq c_{ij} \qquad \forall (i, j) \in E' \tag{4}$$

The objective function—The expression being minimized in (1) reflects the objectives of increasing the total flow in the network, given by $\sum_{ieGen} f_{Si}$, while at the same favoring high-probability interactions via the term $\sum_{ij} -\log(w_{ij}{}^{*} f_{ij}$.

To better explain this second term, suppose that the integer variable x_{ij} indicates the presence of an interaction between node *i* and node *j* in the solution (x_{ij} = 1 if the interaction between node *i* and node *j* is in the solution and x_{ij} = 0 otherwise). Note that minimizing $\sum_{ij} -\log(w_{ij}{}^{*} x_{ij}$ is equivalent to maximizing $\Pi_{ij} w_{ij}{}^{X_{ij}}$, which is the overall probability of all the interactions in the solution for which x_{ij}=1. In the optimization problem given by (1)–(4) above, we allow the x_{ij} variable to take continuous values f_{ij} rather than binary values x_{ij}. This relaxes an integer programming problem, which can be computationally intractable, to a linear programming problem, for which efficient algorithms are available.

The objective function in (1) contains one tunable parameter, γ, which controls the size of the input being connected by ResponseNet, with effective values of 7 to 20 (γ <7 typically results in an empty solution, γ >20 typically saturates the maximum flow attainable). Smaller values of γ identify the subset of input connected by the highest-probability paths. As γ increases additional input components that are connected by lower-probability paths are added. Notably, a change in the tunable parameter values (γ±1) does not typically affect the highest ranking proteins, which provide a skeleton around which the network is built; it does affect the coverage of the input data and consequently determines the inclusion or exclusion of more lowly ranked intermediary proteins (Supplementary Text and Supplementary Figure 8). A protocol for setting γ value appears in the Supplementary text. In the assessment of ResponseNet γ =10 was used because it gave intermediate sized networks.

The constraints—Constraint (2) requires the conservation of flow for each node in the interactome; constraint (3) requires that all flow out of the source must arrive at the sink; constraint (4) enforces that the flow for each interaction is non-negative and does not exceed the capacity of the interaction.

The optimization problem was solved using LOQO [77]. $F = \{f_{ij}>0\}$ was interpreted as a set of weighted interactions that connects the genetic and the transcriptional data sets, defining the predicted response network. This network does not contain proteins and genes from the input sets, except for genetic hits that receive flow from nodes other than the source. Network proteins were ranked in decreasing order according to the total amount of their incoming flow

(calculated for each protein as the sum of the flow value for each incoming edge). Notably, although the solution to the optimization problem is a directed network, the directionality of the interactions in the network, except for the interactions between transcription factors and their targets, was ignored. This directionality only reflects the way in which the algorithm directed flow from the genetic hits to the differentially expressed genes and is not intended to represent the causal order of events (Figure S1 and Supplementary Text).

ResponseNet reports the optimal solution to the flow problem. To map the space of sub-optimal solutions and the stability of the optimal solution we perturbed the edge weights in network and compared the solutions of the perturbed and unperturbed networks. We found that the solution is quite stable even when edge weights are perturbed by a random scaling factor with a mean of one and a standard deviation of 25% (Supplementary Text).

Statistical analysis

Probabilities of overlap between genetic and transcriptional data were calculated using Fisher's Exact Test, based on a total of 6000 yeast genes.

Enrichment analysis was performed using the Gene Ontology Term Finder from SGD. Assessment of ResponseNet on genetic perturbations was based on the subset of 101 genetic perturbations for which the inactivated gene had a reliable GO process annotation (based on direct assays, manual curation or explicit citation, denoted as GO evidence codes IC, IDA or TAS). A specific ResponseNet solution was considered successful when: (i) the predicted network contained the inactivated gene, or (ii) the predicted network was significantly enriched for a biological process to which the inactivated gene was reliably attributed.

Significance was computed against two null hypotheses: (1) relative to the number of genes with the same annotation that could be found by random selection from the genome (p-value $\leq 10^{-2}$ using the hyper-geometric approach and correcting for multiple hypothesis testing), and (2) relative to the enrichment that could be found in 100 perturbation-specific solutions based on randomized inputs (empirical p-value ≤ 0.05). In both cases enrichments were calculated based on genes with reliable process annotation (evidence codes IC, IDA or TAS).

The randomizations were conducted separately for each perturbation as follows: we created 100 pairs of inputs sets of the same sizes as the original genetic and transcriptional data, containing either proteins or genes randomly chosen from the interactome. The interactome data remained fixed so that all predicted networks relied on real interaction data. Each random input set was solved using ResponseNet and the significant GO process annotation enrichments were recorded (p-value $\leq 10^{-2}$ by Fisher's Exact Test; 0.05 FDR). Process annotations enriched in the original solution were considered significant if at least 95 random input solutions had lower significance scores. Interactome data was as described above. Physical interactions relied upon BioGRID release 2.0 [70]. Additional information appears in Supplementary Text.

Yeast Strains and Media

The α-syn overexpressing yeast strain we used in the modifier screen was W303 with α-syn integrated into *HIS3* and *TRP1* loci (IntTox): *MATa can1-100 his3-11,15 leu2-3,112 trp1-1 ura3-1 ade2-1* pRS303Gal-α–synWTYFPpRS304Gal-αSynWT-YFP. The α-syn overexpressing yeast strain we used for drug assays and microarray experiments was W303 with α-syn integrated into *TRP1* and *URA3* loci (HiTox): *MATa can1-100 his3-11,15 leu2-3,112 trp1-1 ura3-1 ade2-1* pRS304Gal-α-synWT-GFP pRS306Gal-α-synWT-GFP. Controls in the drug assays and microarray experiments were W303 with two copies of empty vector integrated into *TRP1* and *URA3* loci (2x vector): *MATa can1-100 his3-11,15 leu2-3,112 trp1-1 ura3-1 ade2-1* pRS304Gal pRS306Gal, and one copy of a-syn integrated into TRP1

locus (1x α-syn): *MATa can1-100 his3-11,15 leu2-3,112 trp1-1 ura3-1 ade2-1* pRS304Gal-α–synWTGFP. The Gal promoter reporter strain used to determine the effect of modifier genes on expression from galactose regulated promoter was W303 with YFP integrated into *HIS3* locus: *MATa can1-100 his3-11,15 leu2-3,112 trp1-1 ura3-1 ade2-1*pRS303Gal-YFP. Strains were manipulated and media prepared using standard techniques.

α–Syn toxicity modifier screen

We performed the high-throughput yeast transformation protocol as described previously for a smaller library of genes [12]. 5,000 full-length yeast ORFs were amplified by polymerase chain reaction and captured by recombination cloning into a Gateway™ pDONR221 vector (Invitrogen). The clones were sequenced from N-terminus to C-terminus and verified to be wild type. For the expression screen, the clones were transfered into a galactose-inducible expression plasmid (pBY011; *CEN*, *URA3*, AmpR) using the Gateway™ technology (Invitrogen). Additional information about the Yeast FLEXGene collection is available at http://www.hip.harvard.edu/research/yeast_flexgene/. Plasmid DNAs from the expression clones were isolated using the REALTM miniprep kit (Qiagen). DNA was dried in individual wells of 96-well microtiter plates and transformed into a strain expressing α–syn integrated at the *HIS3* and *TRP1* loci. A standard lithium acetate transformation protocol was modified for automation and used by employing a BIOROBOT Rapidplate 96-well pipettor (Qiagen). The transformants were grown in synthetic deficient media lacking uracil (SD-Ura) with glucose overnight. The overnight cultures were inoculated into fresh SD-Ura media with raffinose and allowed to reach stationary phase. The cells were spotted on to SD-Ura + glucose and SD-Ura + galactose agar plates. Suppressors of α–syn induced toxicity were identified on galactose plates after 2–3 days of growth at 30°C. We repeated the screen 3 independent times and candidate modifier genes were retested at least twice to confirm their authenticity. To exclude the possibility of false positive toxicity suppressor genes caused simply by a reduction in α–syn expression, the amount of α–syn protein was monitored by flow cytometry. To exclude false positive enhancer genes caused by a general inhibition of growth unrelated to α–syn expression, these genes were transformed into wild type yeast cells and their effect on growth determined.

Immunoblotting

Yeast lysates were subjected to SDS/PAGE (4–12% gradient, Invitrogen) and transferred to a PVDF membrane (Invitrogen). Membranes were blocked with 5% nonfat dry milk in PBS for 1 hr at room temperature. Primary antibody incubations were performed overnight at 4°C or at room temperature for 1–2 hours. After washing with PBS, membranes were incubated with a horseradish peroxidase-conjugated secondary antibody for 1 hour at room temperature, followed by washing in PBS+0.1% Tween 20 (PBST). Proteins were detected with SuperSignal West Dura (Pierce). Phosphoglycerase kinase 1(Pgk 1) mouse monoclonal antibody was used at 1:5000. Hsp26 rabbit polyclonal antibody(gift from Dr. Johannes Buchner) was used at 1:5000. Hsp104 mouse monoclonal antibody (4B; [78]) was used at 1:5000.

α-Syn ResponseNet analysis

The α-syn transcriptional data consisted of genes showing at least a two-fold change in expression with a p-value ≤ 0.05 (Su et al.; manuscript submitted, Supplementary Table 7). ResponseNet was run with γ=12. Capacities of edges connecting the source node to the genetic hits were relative to the absolute strength of the genetic hits (Table 3). Capacities of edges connecting the differentially expressed genes to the sink node were relative to the absolute value of the fold change. In an effort to exclude non-specific stress response from our predictions, we ran ResponseNet with the complete genetic hits data, but using only a subset

of the transcriptional data from which 111 environmental stress response genes [32] were excluded. This resulted in an almost identical network (Supplementary text).

Western blot with S-nitrosocysteine antibody

Yeast cells were harvested, spun down and snap froze prior to cell lysis via bead beating in a buffer containing 50 mM HEPES, pH 7.4, 150 mM NaCl, 1% Triton X-100, 5% glycerol, 1 mM PMSF, and EDTA-free complete protease inhibitor cocktail tablet. Protein concentration was determined via bicinchonic acid assay prior to resolution of products on SDS-PAGE, followed by transfer onto nitrocellulose membrane and probe with S-nitrosocysteine antibody (1:10,000, Sigma).

α-Syn growth in presence of small molecules

α-syn strains as well as control strains were grown overnight to saturation in media containing raffinose. Yeast cultures were normalized for their OD and serially diluted by five-fold prior to spotting onto yeast media plates containing galactose, and where necessary, rapamycin. Growth curves were monitored using Bioscreen (www.bioscreen.fi). Yeast strains were pre-grown in 2% raffinose medium and induced in 2% galactose medium with starting OD_{600} of 0.1. 300 μl of induced cells were dispensed to individual wells, in presence of either the compound or vehicle control (1% DMSO final). Each growth condition was analyzed in triplicate wells per run, and at least 3 independent runs were conducted for each growth condition. Cells were grown at 30°C, with plates shaken every 30 seconds to ensure proper aeration and OD_{600} measurements taken every half hour over a two-day period. The resulting data (OD_{600} versus time) were plotted using Kaleidagraph.

Supplementary Material

Refer to Web version on PubMed Central for supplementary material.

Acknowledgements

E.Y-L has been supported by an EMBO long term post-doctoral fellowship and by a research grant from the National Parkinson Foundation. L.R. has been supported by Roberto Rocca doctoral fellowship and the CSBi Merck-MIT postdoctoral fellowship. L.J.S. was supported by an American Cancer Society postdoctoral fellowship. A.D.G. was a Lilly Fellow of the Life Sciences Research Foundation. M.L.G is supported by a research grant from the National Parkinson Foundation. S.L. is a founder of and has received consulting fees from FoldRx Pharmaceuticals, a company that investigates drugs to treat protein folding diseases. A.D.G. and S.L. are inventors on patents and patent applications that have been licensed to FoldRx. E.F. is the recipient of the Eugene Bell Career Development Chair. This work was supported in part by MGH/MIT Morris Udall Center of Excellence in PD Research NS38372. We thank Mikko Taipale, Sebastian Treusch and Gabriela Caraveo Piso for helpful discussions and comments, and Tom DiCesare for help with figures. L.R. thanks Giorgio Casari and Sergio Cerutti for support and helpful discussions.

References

1. Calvano SE, et al. A network-based analysis of systemic inflammation in humans. Nature 2005;437:1032–1037. [PubMed: 16136080]
2. Haugen AC, et al. Integrating phenotypic and expression profiles to map arsenic-response networks. Genome Biol 2004;5:R95. [PubMed: 15575969]
3. Parsons AB, et al. Integration of chemical-genetic and genetic interaction data links bioactive compounds to cellular target pathways. Nat Biotechnol 2004;22:62–69. [PubMed: 14661025]
4. Begley TJ, Rosenbach AS, Ideker T, Samson LD. Hot spots for modulating toxicity identified by genomic phenotyping and localization mapping. Mol Cell 2004;16:117–125. [PubMed: 15469827]
5. Deutschbauer AM, Williams RM, Chu AM, Davis RW. Parallel phenotypic analysis of sporulation and postgermination growth in Saccharomyces cerevisiae. Proc Natl Acad Sci U S A 2002;99:15530–15535. [PubMed: 12432101]

6. Fry RC, Begley TJ, Samson LD. Genome-wide responses to DNA-damaging agents. Annu Rev Microbiol 2005;59:357–377. [PubMed: 16153173]
7. Birrell GW, et al. Transcriptional response of Saccharomyces cerevisiae to DNA-damaging agents does not identify the genes that protect against these agents. Proc Natl Acad Sci U S A 2002;99:8778–8783. [PubMed: 12077312]
8. Winzeler EA, et al. Functional characterization of the S. cerevisiae genome by gene deletion and parallel analysis. Science 1999;285:901–906. [PubMed: 10436161]
9. Smith JJ, et al. Expression and functional profiling reveal distinct gene classes involved in fatty acid metabolism. Mol Syst Biol 2006;22006 0009
10. Schiesling C, Kieper N, Seidel K, Kruger R. Review: Familial Parkinson's disease--genetics, clinical phenotype and neuropathology in relation to the common sporadic form of the disease. Neuropathol Appl Neurobiol 2008;34:255–271. [PubMed: 18447897]
11. Outeiro TF, Lindquist S. Yeast cells provide insight into alpha-synuclein biology and pathobiology. Science 2003;302:1772–1775. [PubMed: 14657500]
12. Cooper AA, et al. Alpha-synuclein blocks ER-Golgi traffic and Rab1 rescues neuron loss in Parkinson's models. Science 2006;313:324–328. [PubMed: 16794039]
13. Workman CT, et al. A systems approach to mapping DNA damage response pathways. Science 2006;312:1054–1059. [PubMed: 16709784]
14. Beyer A, Bandyopadhyay S, Ideker T. Integrating physical and genetic maps: from genomes to interaction networks. Nat Rev Genet 2007;8:699–710. [PubMed: 17703239]
15. Yeang CH, Ideker T, Jaakkola T. Physical network models. J Comput Biol 2004;11:243–262. [PubMed: 15285891]
16. Ourfali O, Shlomi T, Ideker T, Ruppin E, Sharan R. SPINE: a framework for signaling-regulatory pathway inference from cause-effect experiments. Bioinformatics 2007;23:i359–i366. [PubMed: 17646318]
17. Dasika MS, Burgard A, Maranas CD. A computational framework for the topological analysis and targeted disruption of signal transduction networks. Biophys J 2006;91:382–398. [PubMed: 16617070]
18. Cormen TH, Leiserson CE, Rivest RL, Stein C. Introduction to Algorithms. 2001
19. SGD project. “Saccharomyces Genome Database”.
20. Hughes TR, et al. Functional discovery via a compendium of expression profiles. Cell 2000;102:109–126. [PubMed: 10929718]
21. Chang M, Bellaoui M, Boone C, Brown GW. A genome-wide screen for methyl methanesulfonate-sensitive mutants reveals genes required for S phase progression in the presence of DNA damage. Proc Natl Acad Sci U S A 2002;99:16934–16939. [PubMed: 12482937]
22. Gasch AP, et al. Genomic expression responses to DNA-damaging agents and the regulatory role of the yeast ATR homolog Mec1p. Mol Biol Cell 2001;12:2987–3003. [PubMed: 11598186]
23. Tofaris GK, Spillantini MG. Physiological and pathological properties of alpha-synuclein. Cell Mol Life Sci 2007;64:2194–2201. [PubMed: 17605001]
24. Spillantini MG, et al. Alpha-synuclein in Lewy bodies. Nature 1997;388:839–840. [PubMed: 9278044]
25. Polymeropoulos MH, et al. Mutation in the alpha-synuclein gene identified in families with Parkinson's disease. Science 1997;276:2045–2047. [PubMed: 9197268]
26. Singleton AB, et al. alpha-Synuclein locus triplication causes Parkinson's disease. Science 2003;302:841. [PubMed: 14593171]
27. Lee VM, Trojanowski JQ. Mechanisms of Parkinson's disease linked to pathological alpha-synuclein: new targets for drug discovery. Neuron 2006;52:33–38. [PubMed: 17015225]
28. Gitler AD, et al. The Parkinson's disease protein alpha-synuclein disrupts cellular Rab homeostasis. Proc Natl Acad Sci U S A 2008;105:145–150. [PubMed: 18162536]
29. Schapira AH. Mitochondria in the aetiology and pathogenesis of Parkinson's disease. Lancet Neurol 2008;7:97–109. [PubMed: 18093566]

30. Sarkar S, Davies JE, Huang Z, Tunnacliffe A, Rubinsztein DC. Trehalose, a novel mTOR-independent autophagy enhancer, accelerates the clearance of mutant huntingtin and alpha-synuclein. J Biol Chem 2007;282:5641–5652. [PubMed: 17182613]

31. Olanow CW. Manganese-induced parkinsonism and Parkinson's disease. Ann N Y Acad Sci 2004;1012:209–223. [PubMed: 15105268]

32. Gasch AP, et al. Genomic expression programs in the response of yeast cells to environmental changes. Mol Biol Cell 2000;11:4241–4257. [PubMed: 11102521]

33. Dawson TM. Parkin and defective ubiquitination in Parkinson's disease. J Neural Transm Suppl 2006:209–213. [PubMed: 17017531]

34. Staropoli JF, et al. Parkin is a component of an SCF-like ubiquitin ligase complex and protects postmitotic neurons from kainate excitotoxicity. Neuron 2003;37:735–749. [PubMed: 12628165]

35. West AB, Dawson VL, Dawson TM. To die or grow: Parkinson's disease and cancer. Trends Neurosci 2005;28:348–352. [PubMed: 15913799]

36. Hoglinger GU, et al. The pRb/E2F cell-cycle pathway mediates cell death in Parkinson's disease. Proc Natl Acad Sci U S A 2007;104:3585–3590. [PubMed: 17360686]

37. Sarver A, DeRisi J. Fzf1p regulates an inducible response to nitrosative stress in Saccharomyces cerevisiae. Mol Biol Cell 2005;16:4781–4791. [PubMed: 16014606]

38. Uehara T, et al. S-nitrosylated protein-disulphide isomerase links protein misfolding to neurodegeneration. Nature 2006;441:513–517. [PubMed: 16724068]

39. Almeida B, et al. NO-mediated apoptosis in yeast. J Cell Sci 2007;120:3279–3288. [PubMed: 17726063]

40. Mandemakers W, Morais VA, De Strooper B. A cell biological perspective on mitochondrial dysfunction in Parkinson disease and other neurodegenerative diseases. J Cell Sci 2007;120:1707–1716. [PubMed: 17502481]

41. Martin LJ, et al. Parkinson's disease alpha-synuclein transgenic mice develop neuronal mitochondrial degeneration and cell death. J Neurosci 2006;26:41–50. [PubMed: 16399671]

42. Liu Z, Spirek M, Thornton J, Butow RA. A novel degron-mediated degradation of the RTG pathway regulator, Mks1p, by SCFGrr1. Mol Biol Cell 2005;16:4893–4904. [PubMed: 16093347]

43. Zou J, Guo Y, Guettouche T, Smith DF, Voellmy R. Repression of heat shock transcription factor HSF1 activation by HSP90 (HSP90 complex) that forms a stress-sensitive complex with HSF1. Cell 1998;94:471–480. [PubMed: 9727490]

44. Flower TR, Chesnokova LS, Froelich CA, Dixon C, Witt SN. Heat shock prevents alpha-synuclein-induced apoptosis in a yeast model of Parkinson's disease. J Mol Biol 2005;351:1081–1100. [PubMed: 16051265]

45. Auluck PK, Meulener MC, Bonini NM. Mechanisms of Suppression of {alpha}-Synuclein Neurotoxicity by Geldanamycin in Drosophila. J Biol Chem 2005;280:2873–2878. [PubMed: 15556931]

46. Lin JT, Lis JT. Glycogen synthase phosphatase interacts with heat shock factor to activate CUP1 gene transcription in Saccharomyces cerevisiae. Mol Cell Biol 1999;19:3237–3245. [PubMed: 10207049]

47. Hickman MJ, Winston F. Heme levels switch the function of Hap1 of Saccharomyces cerevisiae between transcriptional activator and transcriptional repressor. Mol Cell Biol 2007;27:7414–7424. [PubMed: 17785431]

48. Duennwald ML, Jagadish S, Muchowski PJ, Lindquist S. Flanking sequences profoundly alter polyglutamine toxicity in yeast. Proc Natl Acad Sci U S A 2006;103:11045–11050. [PubMed: 16832050]

49. Ravikumar B, et al. Inhibition of mTOR induces autophagy and reduces toxicity of polyglutamine expansions in fly and mouse models of Huntington disease. Nat Genet 2004;36:585–595. [PubMed: 15146184]

50. Khurana V, et al. TOR-mediated cell-cycle activation causes neurodegeneration in a Drosophila tauopathy model. Curr Biol 2006;16:230–241. [PubMed: 16461276]

51. Kelley R, Ideker T. Systematic interpretation of genetic interactions using protein networks. Nat Biotechnol 2005;23:561–566. [PubMed: 15877074]

52. Schuldiner M, et al. Exploration of the function and organization of the yeast early secretory pathway through an epistatic miniarray profile. Cell 2005;123:507–519. [PubMed: 16269340]
53. Yeger-Lotem E, et al. Network motifs in integrated cellular networks of transcription-regulation and protein-protein interaction. Proc Natl Acad Sci U S A 2004;101:5934–5939. [PubMed: 15079056]
54. Zhao R, et al. Navigating the chaperone network: an integrative map of physical and genetic interactions mediated by the hsp90 chaperone. Cell 2005;120:715–727. [PubMed: 15766533]
55. Ulitsky I, Shlomi T, Kupiec M, Shamir R. From E-MAPs to module maps: dissecting quantitative genetic interactions using physical interactions. Mol Syst Biol 2008;4:209. [PubMed: 18628749]
56. Deutscher D, Meilijson I, Kupiec M, Ruppin E. Multiple knockout analysis of genetic robustness in the yeast metabolic network. Nat Genet 2006;38:993–998. [PubMed: 16941010]
57. Holstege FC, et al. Dissecting the regulatory circuitry of a eukaryotic genome. Cell 1998;95:717–728. [PubMed: 9845373]
58. Santos SD, Verveer PJ, Bastiaens PI. Growth factor-induced MAPK network topology shapes Erk response determining PC-12 cell fate. Nat Cell Biol 2007;9:324–330. [PubMed: 17310240]
59. Goehler H, et al. A protein interaction network links GIT1, an enhancer of huntingtin aggregation, to Huntington's disease. Mol Cell 2004;15:853–865. [PubMed: 15383276]
60. Pujana MA, et al. Network modeling links breast cancer susceptibility and centrosome dysfunction. Nat Genet 2007;39:1338–1349. [PubMed: 17922014]
61. Lim J, et al. A protein-protein interaction network for human inherited ataxias and disorders of Purkinje cell degeneration. Cell 2006;125:801–814. [PubMed: 16713569]
62. Said MR, Begley TJ, Oppenheim AV, Lauffenburger DA, Samson LD. Global network analysis of phenotypic effects: protein networks and toxicity modulation in Saccharomyces cerevisiae. Proc Natl Acad Sci U S A 2004;101:18006–18011. [PubMed: 15608068]
63. Shachar R, Ungar L, Kupiec M, Ruppin E, Sharan R. A systems-level approach to mapping the telomere length maintenance gene circuitry. Mol Syst Biol 2008;4:172. [PubMed: 18319724]
64. Bromberg KD, Ma'ayan A, Neves SR, Iyengar R. Design logic of a cannabinoid receptor signaling network that triggers neurite outgrowth. Science 2008;320:903–909. [PubMed: 18487186]
65. Tu Z, Wang L, Arbeitman MN, Chen T, Sun F. An integrative approach for causal gene identification and gene regulatory pathway inference. Bioinformatics 2006;22:e489–e496. [PubMed: 16873511]
66. Suthram S, Beyer A, Karp RM, Eldar Y, Ideker T. eQED: an efficient method for interpreting eQTL associations using protein networks. Mol Syst Biol 2008;4:162. [PubMed: 18319721]
67. Silva JM, et al. Profiling essential genes in human mammary cells by multiplex RNAi screening. Science 2008;319:617–620. [PubMed: 18239125]
68. Huang X, et al. Lower low-density lipoprotein cholesterol levels are associated with Parkinson's disease. Mov Disord 2007;22:377–381. [PubMed: 17177184]
69. Huang X, Abbott RD, Petrovitch H, Mailman RB, Ross GW. Low LDL cholesterol and increased risk of Parkinson's disease: prospective results from Honolulu-Asia Aging Study. Mov Disord 2008;23:1013–1018. [PubMed: 18381649]
70. Reguly T, et al. Comprehensive curation and analysis of global interaction networks in Saccharomyces cerevisiae. J Biol 2006;5:11. [PubMed: 16762047]
71. Mewes HW, et al. MIPS: a database for genomes and protein sequences. Nucleic Acids Res 2002;30:31–34. [PubMed: 11752246]
72. MacIsaac KD, et al. An improved map of conserved regulatory sites for Saccharomyces cerevisiae. BMC Bioinformatics 2006;7:113. [PubMed: 16522208]
73. Milo R, et al. Network motifs: simple building blocks of complex networks. Science 2002;298:824–827. [PubMed: 12399590]
74. Harbison CT, et al. Transcriptional regulatory code of a eukaryotic genome. Nature 2004;431:99–104. [PubMed: 15343339]
75. Myers CL, et al. Discovery of biological networks from diverse functional genomic data. Genome Biol 2005;6:R114. [PubMed: 16420673]
76. Hoffmann R, Valencia A. Life cycles of successful genes. Trends Genet 2003;19:79–81. [PubMed: 12547515]

77. Vanderbei RJ. LOQO User's Manual--Version 3.10. Optimization Methods and Software 1999;12:485–514.

78. Cashikar AG, et al. Defining a pathway of communication from the C-terminal peptide binding domain to the N-terminal ATPase domain in a AAA protein. Mol Cell 2002;9:751–760. [PubMed: 11983167]

79. Dudley AM, Janse DM, Tanay A, Shamir R, Church GM. A global view of pleiotropy and phenotypically derived gene function in yeast. Mol Syst Biol 2005;12005 0001

80. Koerkamp MG, et al. Dissection of transient oxidative stress response in Saccharomyces cerevisiae by using DNA microarrays. Mol Biol Cell 2002;13:2783–2794. [PubMed: 12181346]

81. Tong AH, et al. Systematic genetic analysis with ordered arrays of yeast deletion mutants. Science 2001;294:2364–2368. [PubMed: 11743205]

82. Tong AH, et al. Global mapping of the yeast genetic interaction network. Science 2004;303:808–813. [PubMed: 14764870]

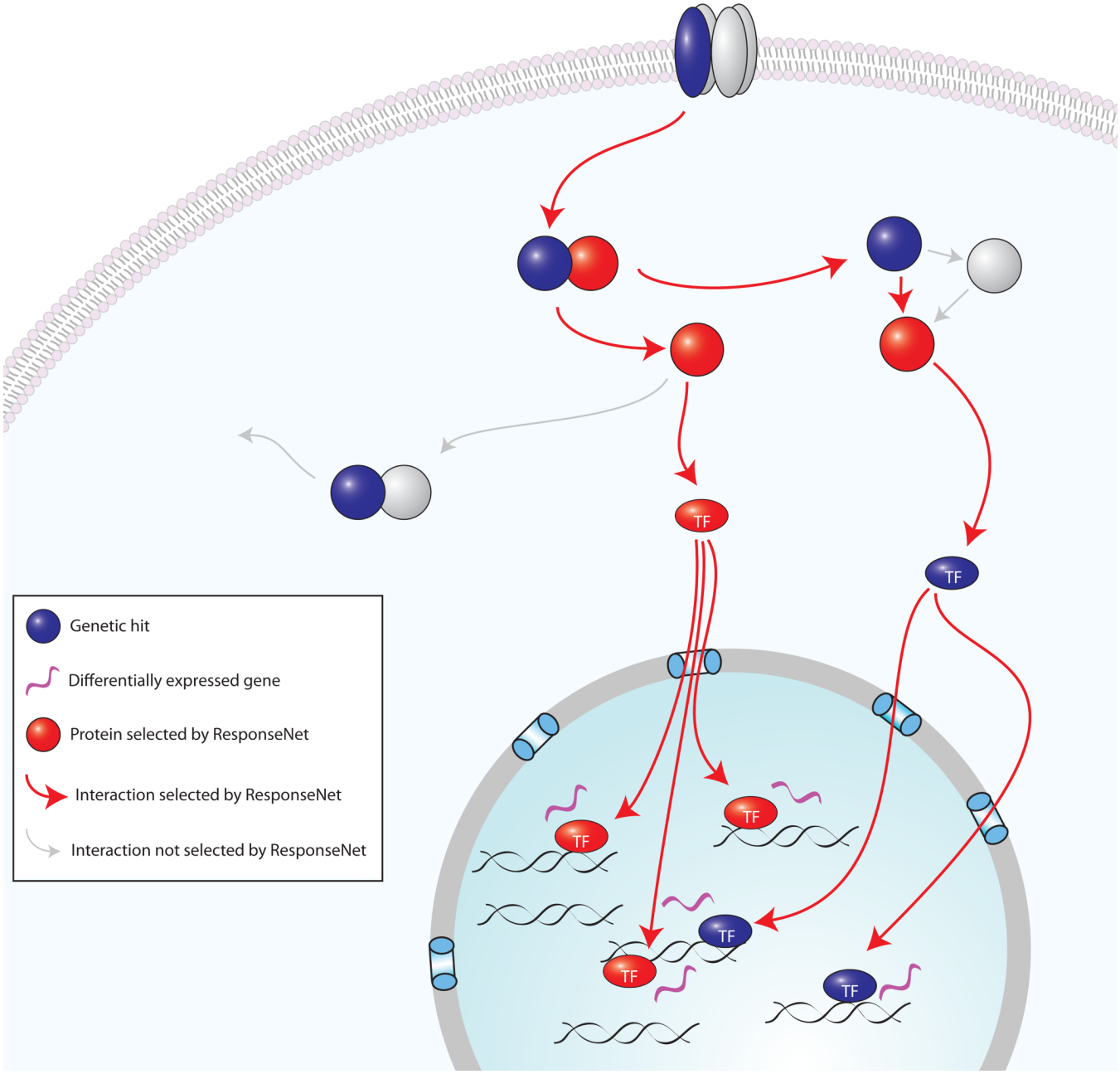

Figure 1. Regulatory relationships between stimulus-specific genetic and transcriptional data

Cells respond to stimulus with changes in many cellular processes, including signaling and gene expression. The figure shows a general signaling pathway, including receptor binding, transcription factor (TF) translocation into the nucleus and gene expression. Genetic screens and mRNA profiling identify only some of these molecular components and often do not identify the same genes, as shown. We find that the proteins products of genes identified in genetic screens (colored blue) tend to be molecules with regulatory roles. We therefore hypothesize that they may directly or indirectly contribute to the regulation of the observed change in gene expression (colored purple). ResponseNet identifies the likely regulatory pathways, and predicts proteins that are part of these pathways even if they are not identified in either screen (colored red).

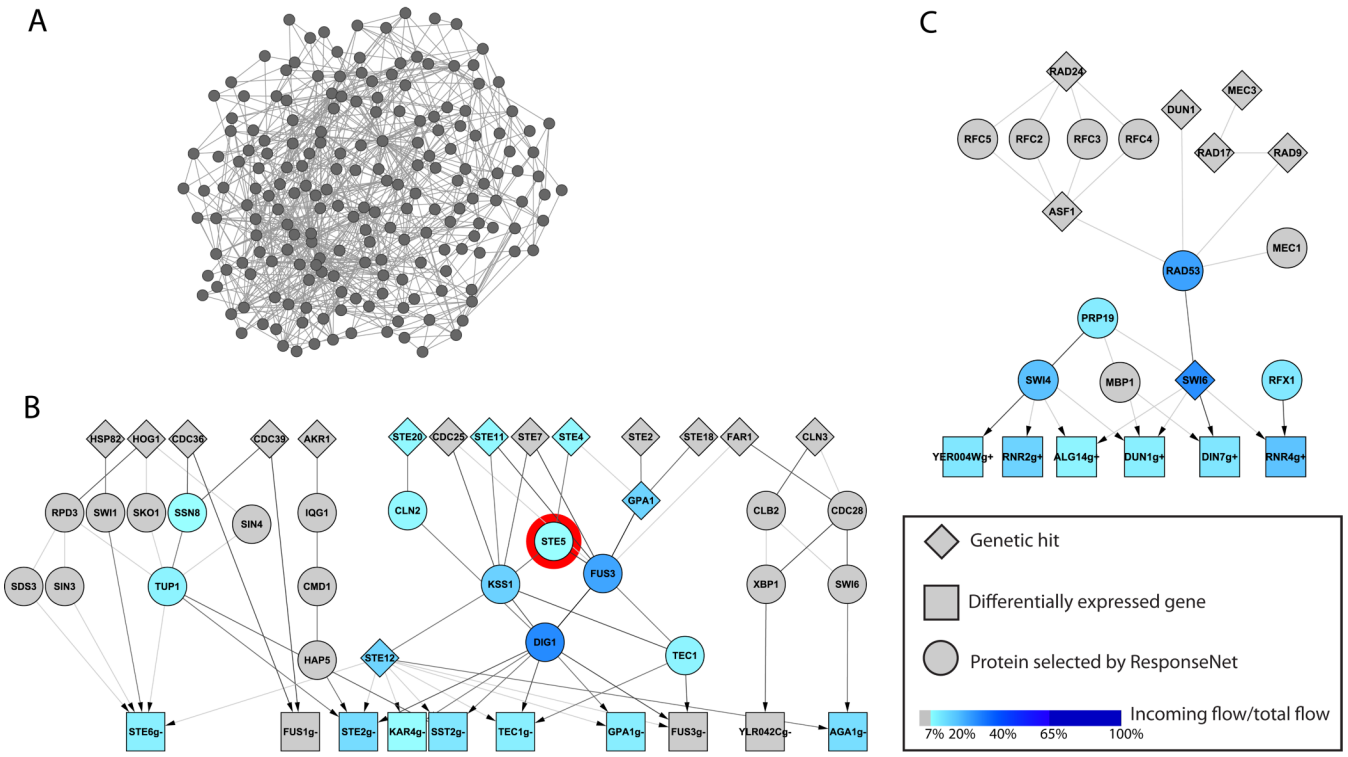

Figure 2. Interactome sub-networks connecting genetic and transcriptional data

A. A network connecting genetic[19] and transcriptional[20] data of STE5 deletion strain via paths of length ≤ 3 edges finds 193 nodes and 778 edges.

B. The network created by ResponseNet connects the genetic[19] and transcriptional[20] data of STE5 deletion strain via 23 intermediary nodes and 96 edges. Higher ranked nodes, as determined by ResponseNet, appear in darker shades of blue and include core components of the pheromone response pathway. Ste5 itself, marked by a red circle, is ranked ninth among the top predicted proteins.

C. The highly-ranked part of the network created by ResponseNet upon connecting genetic hits[4,21] to DNA damage signature genes[22] identified in yeast treated with the DNA damaging agent MMS. The highest ranking intermediate nodes predicted by ResponseNet include core components of the DNA damage response pathway. The complete network appears in Supplementary Figure 7.

Each node represents either a protein or a gene, and edges represent protein-protein, metabolic, and protein-DNA interactions. The darkness of an edge increases with the amount of flow it carries. Differentially expressed genes are labeled with a suffix of g+ for up- and g- for down-regulation. Networks were visualized using Cytoscape.

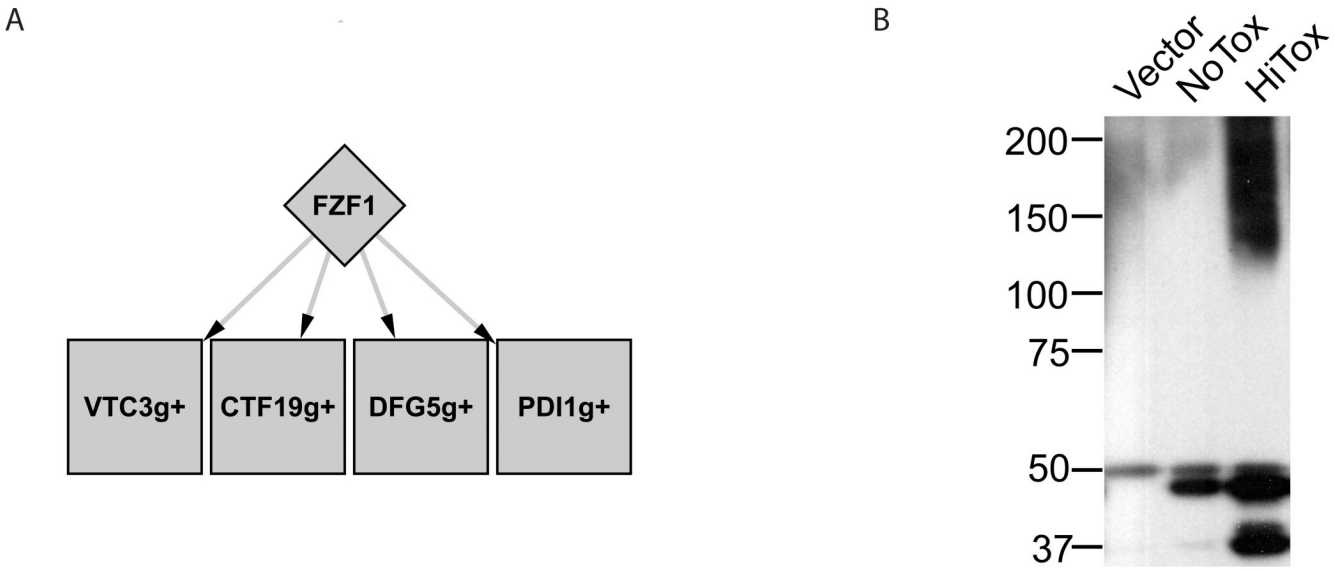

Figure 3. Nitrosative stress response to α-syn expression in yeast

A. The predicted sub-network containing Fzf1 and its differentially expressed target genes. Graphical representation is similar to Figure 2.

B. Immunoblotting against S-nitrosocysteine performed on a control strain (vector), on a strain expressing one copy of α-syn (NoTox), and on a high-toxicity strain (HiTox) expressing several copies of α-syn, reveals that increasing levels of α-syn increase the amount of S-nitrosylated proteins.

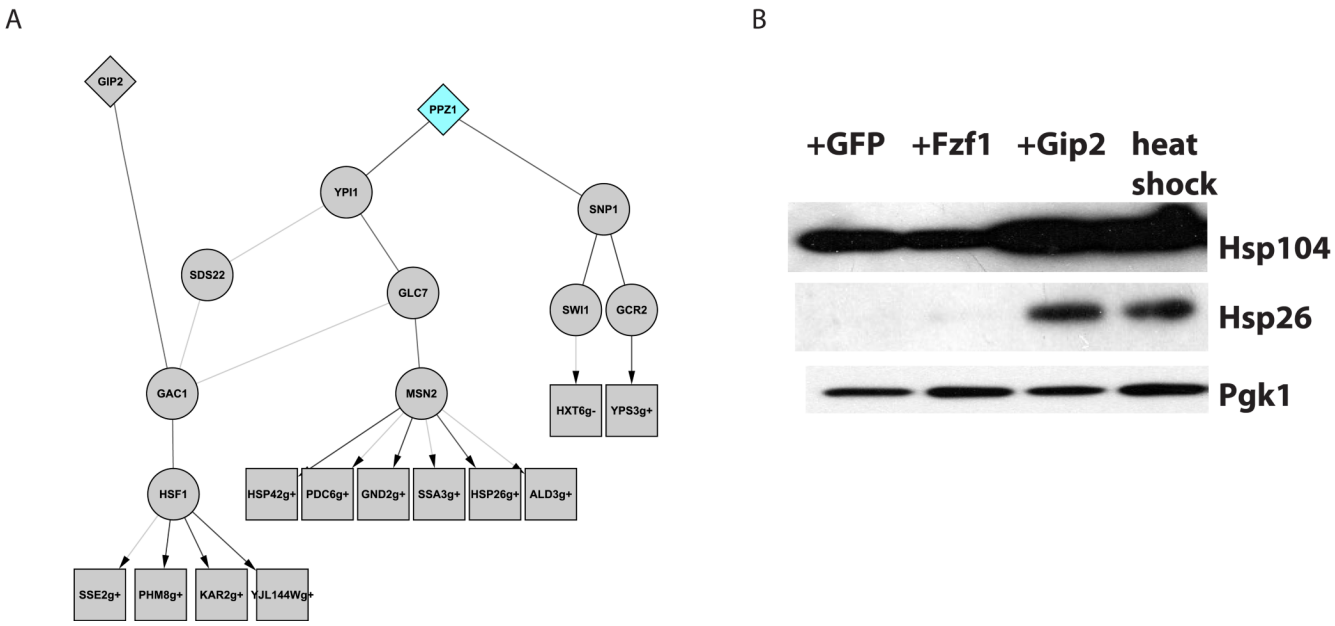

Figure 4. Overexpression of Gip2 causes induced expression of Hsf1 targets

A. The predicted sub-network links the toxicity suppressor Gip2 and the toxicity enhancer Ppz1 to Hsf1 and Msn2 via components of type 1 protein phosphatase complex (Gac1, Glc7, Ypi1, Sds22). Graphical representation is similar to Figure 2.

B. Immunoblotting of vector cells overexpressing GFP, Fzf1 or Gip2 with antibodies against Hsp104 and Hsp26. Overexpression of Gip2 is sufficient to activate Hsf1 and induce higher protein levels of both its targets Hsp104 and Hsp26, similar to that of vector cells subjected to heat shock. In contrast, ovexepression of another genetic suppressor, Fzf1, does not activate Hsf1. Immunoblotting against Pgk1 was used as a loading control.

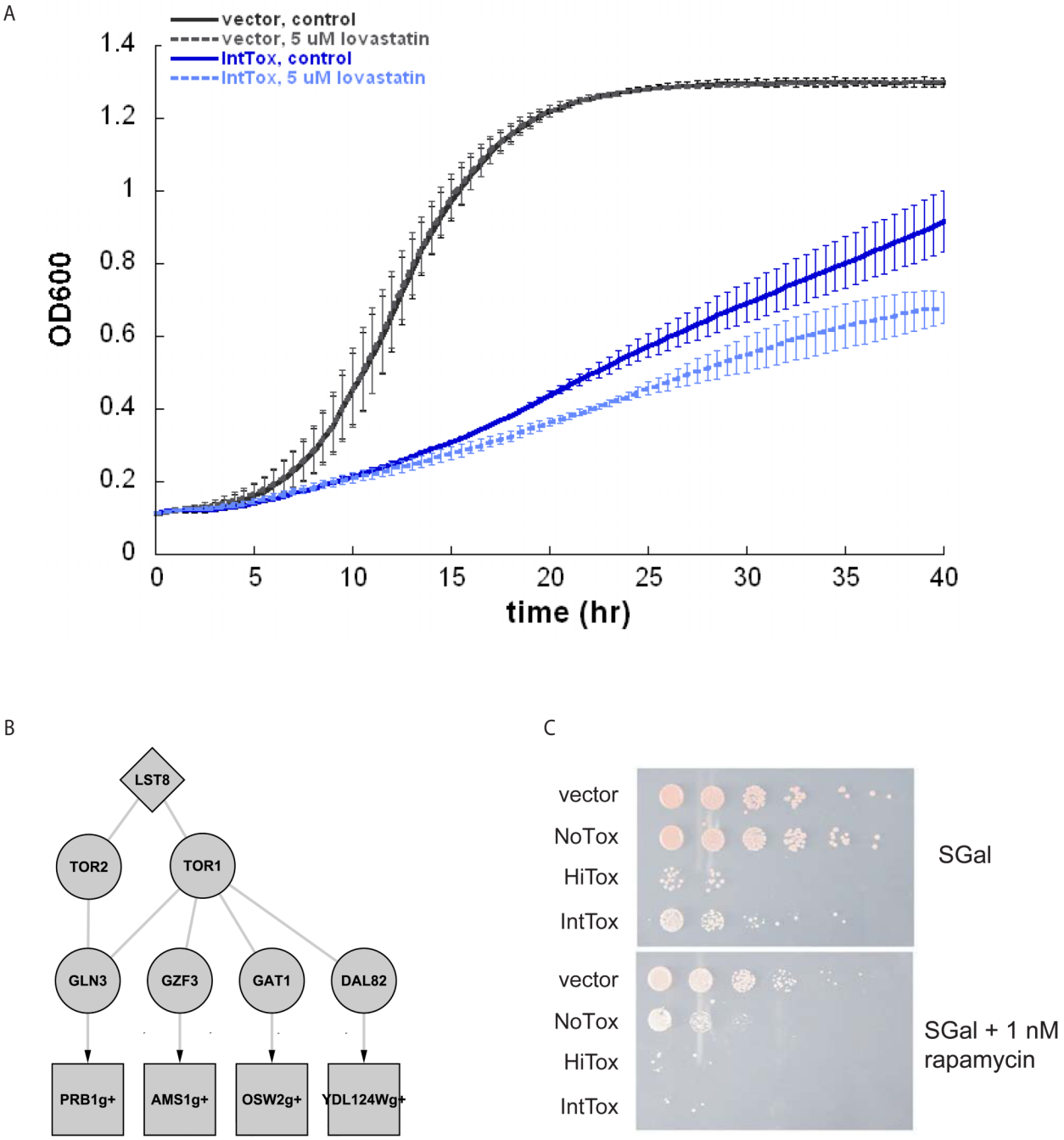

Figure 5. Effects of the small molecules lovastatin and rapamycin on α-syn toxicity

A. Lovastatin inhibits growth of the yeast strain expressing an intermediate level of α-syn. Growth of a control strain (vector) and an intermediate toxicity strain (IntTox) expressing several copies of α-syn was measured in a galactose containing media with and without 5μM lovastatin. Each growth curve reflects the average of 3 individual runs, each of which is indicated by a bar.

B. The predicted sub-network containing TOR pathway components includes the predicted proteins Tor1 and Tor2. Graphical representation is similar to Figure 2.

C. The effect of rapamycin on growth of different yeast strains. The upper panel shows the growth of a control strain (vector), a strain expressing one copy of α- syn (NoTox), a high-

toxicity strain (HiTox) and an intermediate toxicity strain (IntTox) both expressing several copies of α-syn, in a galactose containing media (SGal) that is used to induce expression of α-syn. The lower panel shows the same strains grown in media that also contains 1nM rapamycin, showing that rapamycin inhibits growth of all α-syn expressing strains but not the control strain, as observed by the difference in the number of colonies per drop. The different columns correspond to serial dilutions.

Table 1

Measured responses to cellular perturbations.

Perturbation	Number of differentially expressed genes[1]	Number of genetic hits[2]	Overlap
Growth arrest (HU) [20,79]	59	86	0
DNA damage (MMS) [4,13]	198	1448	43
ER stress (tunicamycin) [3,20]	200	127	5
Fatty acid metabolism (oleate) [9,80]	269	103	9
ATP synthesis block (arsenic)[2]	828	50	9
Protein biosynthesis (cycloheximide) [20,79]	20	164	0
Gene inactivation, screen complete (24 data sets [19,20,81,82])[3]	27	130	0
Gene inactivation, screen incomplete (149 data sets [19,20])[3]	24	12	0

[1] Differentially expressed genes were defined as those showing at least a 2-fold change in expression following the perturbation or as defined in the original papers.

[2] Number of genes whose genetic manipulation affects the phenotype of perturbed cells relative to wild type.

[3] Median results are shown.

Table 2

Assessment of the ResponseNet algorithm using 101 gene inactivation perturbations.

Source of genetic hits data	Number of genetic data sets	Median number of predicted proteins	Success in predicting inactivated gene		Success in predicting inactivated gene process	Success in predicting inactivated gene or its process
			% predicted	% predicted in top 20		
Synthetic genetic arrays (complete screen)	15	102	33	13	67%	67%
Literature (incomplete data)	86	61	33	27	53%	62%
Total	101	64	33	25	56%	63%

Table 3

Yeast genes that modify α-syn toxicity when overexpressed.

Yeast Gene	Type	Strength	Human ortholog(s)	Proposed function
		Amino Acid Transport		
AVT4	suppressor	3	SLC36A1 SLC36A2 SLC36A3 SLC36A4	Vacuolar transporter; exports large neutral amino acids from the vacuole
DIP5	suppressor	3	SLC7A1 SLC7A14 SLC7A2 SLC7A3 SLC7A4 SLC7A13	Dicarboxylic amino acid permease
LST8	suppressor	3	GBL	Component of the TOR signaling pathway
		Autophagy		
NVJ1	suppressor	2		Nuclear envelope protein; functions during piecemeal microautophagy of the nucleus (PMN)
		Cytoskeleton		
ICY1	suppressor	4		Protein that interacts with the cytoskeleton
ICY2	suppressor	4		Protein that interacts with the cytoskeleton
		Manganese transport		
CCC1	suppressor	4		Putative vacuolar Fe2+/Mn2+ transporter
PMR1	enhancer	−7	ATP2C1 ATP2C2	High affinity Ca2+/Mn2+ P-type ATPase required for Ca2+ and Mn2+ transport into Golgi
		Protein phosphorylation		
IME2	suppressor	4	ICK	Serine/threonine protein kinase involved in activation of meiosis

Yeast Gene	Type	Strength	Human ortholog(s)	Proposed function
PTP2	suppressor	3	PTPRE, PTPRC, PTPN22, PTPRG	Phosphotyrosine-specific protein phosphatase involved in osmolarity sensing
GIP2	suppressor	3	PPP1R3A PPP1R3B PPP1R3C PPP1R3D PPP1R3E	Putative regulatory subunit of the protein phosphatase Glc7p, involved in glycogen metabolism
YCK3	suppressor	3	CSNK1G1 CSNK1G2 CSNK1G3	Palmitoylated, vacuolar membranelocalized casein kinase I isoform
RCK1	suppressor	3	CAMK1G	Protein kinase involved in the response to oxidative stress
CDC5	suppressor (Cdc5 overexpression is toxic; in presence of a-syn it rescues/ rescued)	3	PLK2	Polo-like kinase; found at bud neck, nucleus and SPBs; has multiple functions in mitosis and cytokinesis
PTC4	suppressor	1	PPM1G	Cytoplasmic type 2C protein phosphatase
SIT4	enhancer	−2	PPP6C	Type 2A-related serine-threonine phosphatase.
CAX4	enhancer	−3	DOLPP1	Dolichyl pyrophosphate phosphatase, required for Dol-P-P-linked oligosaccharide intermediate synthesis and protein N-glycosylation.
PPZ2	enhancer	−3	PPP1CC PPP1CB PPP1CA	Serine/threonine protein phosphatase Z
PPZ1	enhancer	−8	PPP1CA PPP1CB PPP1CC	Serine/threonine protein phosphatase Z
		Transcription/Translation		
CUP9	suppressor	3	MEIS1 MEIS2 MEIS3 NR_002211	Transcriptional repressor involved in copper ion homeostasis

Yeast Gene	Type	Strength	Human ortholog(s)	Proposed function
			.1 PKNOX1 PKNOX2 Q99687-3 TGIF1 TGIF2 TGIF2LX	
HAP4	suppressor	4		Transcriptional activator and global regulator of respiratory gene expression
FZF1	suppressor	3	KLF15 KLF11 ZNF624	Key transcriptional regulator of cellular response to nitrosative stress
MGA2	suppressor	3	ANKRD1 OSBPL1A	ER membrane protein involved in regulation of OLE1 transcription
MKS1	enhancer	−5		Pleiotropic negative transcriptional regulator involved in Ras-CAMP and lysine biosynthetic pathways and nitrogen regulation; involved in retrograde (RTG) mitochondria-to-nucleus signaling
VHR1	suppressor	3		Transcriptional activator
JSN1	suppressor	2	PUM1	Member of the Puf family of RNAbinding proteins, interacts with mRNAs encoding membrane-associated proteins
SUT2	enhancer	−3		Putative transcription factor; multicopy suppressor of mutations that cause low activity of the cAMP/protein kinase A pathway
TIF4632	suppressor	3	EIF4G1 EIF4G2 EIF4G3	Translation initiation factor eIF4G, subunit of the mRNA cap-binding protein complex (eIF4F)
STB3	suppressor	3		Protein that binds Sin3p in a two-hybrid assay.
MATALPHA1	enhancer	−5		Transcriptional co-activator involved in regulation of mating-type-specific gene expression
		Trehalose biosynthesis		

Yeast Gene	Type	Strength	Human ortholog(s)	Proposed function
UGP1	suppressor	4	UGP2	UDP-glucose pyrophosphorylase, catalyses the formation of UDP-Glc, a precursor to trehalose
TPS3	suppressor	3		Regulatory subunit of trehalose-6-phosphate synthase/phosphatase complex, which synthesizes trehalose
NTH1	suppressor	2	TREH	Neutral trehalase, degrades trehalose; required for thermotolerance and may mediate resistance to other cellular stresses
		Ubiquitin-related		
CDC4	suppressor	4	FBXW7	F-box, associates with Skp1p and Cdc53p to form a complex, SCFCdc4, which acts as ubiquitin-protein ligase
UIP5	suppressor	4		Protein of unknown function that interacts with Ulp1p, a Ubl (ubiquitin-like protein)-specific protease
HRD1	suppressor	4	AMFR SYVNI	Ubiquitin-protein ligase required for endoplasmic reticulum-associated degradation (ERAD) of misfolded proteins
UBP11	enhancer	−3	USP21	Ubiquitin-specific protease that cleaves ubiquitin from ubiquitinated proteins.
UBP7	enhancer	−4	USP21	Ubiquitin-specific protease that cleaves ubiquitin-protein fusions.
		Vesicular transport, ER-Golgi		
YPT1	suppressor	5	RAB10 RAB13 RAB1A RAB1C RAB8A RAB8B	Ras-like small GTPase, involved in the ER-to-Golgi step of the secretory pathway
YKT6	suppressor	4	YKT6	v-SNARE involved in trafficking to and within the Golgi, endocytic trafficking to the vacuole, and vacuolar fusion
BRE5	suppressor	4	G3BP2	Ubiquitin protease cofactor, forms deubiquitination complex with Ubp3p to regulate ER-Golgi transport

Yeast Gene	Type	Strength	Human ortholog(s)	Proposed function
SEC21	suppressor	4	COPG2 COPG	Gamma subunit of coatomer, a heptameric protein complex that together with Arf1p forms the COPI coat
UBP3	suppressor	3	USP10	Ubiquitin-specific protease that interacts with Bre5p to co-regulate anterograde and retrograde transport between ER and Golgi
ERV29	suppressor	3	SURF4	Protein localized to COPII-coated vesicles, involved in vesicle formation and incorporation of specific secretory cargo.
SEC28	suppressor	3	COPE	Epsilon-COP subunit of the coatomer; regulates retrograde Golgi-to-ER protein traffic; stabilizes Cop1p
SFT1	suppressor	2	mouse BET1	Intra-Golgi v-SNARE, required for transport of proteins between an early and a later Golgi compartment.
GLO3	enhancer	−1	ARFGAP3 ZNF289	ADP-ribosylation factor GTPase activating protein (ARF GAP), involved in ER-Golgi transport
TRS120	enhancer	−2	NIBP	One of 10 subunits of the transport protein particle (TRAPP) complex of the cis-Golgi which mediates vesicle docking and fusion
GYP8	enhancer	−2	TBC1D20	GTPase-activating protein for yeast Rab family members; Ypt1p is the preferred in vitro substrate
YIP3	enhancer	−2	RABAC1	Protein localized to COPII vesicles, proposed to be involved in ER to Golgi transport; interacts with Rab GTPases
BET4	enhancer	−3	RABGGTA	Alpha subunit of Type II geranylgeranyltransferase; provides a membrane attachment moiety to Rab-like proteins Ypt1p and Sec4p
SLY41	enhancer	−5	SLC35E1	Protein involved in ER-to-Golgi transport.
GOS1	enhancer	−2	GOSR1	v-SNARE protein involved in Golgi transport, homolog of the mammalian protein GOS-28/GS28
SEC31	enhancer	−2	SEC31A SEC31B	Essential phosphoprotein component (p150) of the COPII coat of secretory pathway vesicles, in complex with

Yeast Gene	Type	Strength	Human ortholog(s)	Proposed function
				Sec13p; required for ER-derived transport vesicle formation
		Other cellular processes		
PFS1	suppressor	4		Sporulation protein required for prospore membrane formation at selected spindle poles
PDE2	suppressor	4	PDE10A PDE11A PDE1A PDE1B PDE1C PDE2A PDE3A PDE3B PDE4A PDE4B PDE4C PDE4D PDE5A PDE6A PDE6B PDE6C PDE7A PDE7B PDE8A PDE8B PDE9A	High-affinity cyclic AMP phosphodiesterase, component of the cAMP-dependent protein kinase signaling system
MUM2	suppressor	4		Interacts with Orc2p, which is a component of the origin recognition complex.
OSH3	suppressor	3	OSBPL1A OSBPL2 OSBPL3 OSBPL6 OSBPL7	Member of an oxysterol-binding protein family, functions in sterol metabolism
PHO80	suppressor	3		Cyclin, negatively regulates phosphate metabolism
OSH2	suppressor	3	OSBPL3 OSBP OSBP2	Member of an oxysterol-binding protein family, functions in sterol metabolism

Yeast Gene	Type	Strength	Human ortholog(s)	Proposed function
ISN1	suppressor	2		Inosine 5′-monophosphate (IMP)-specific 5′-nucleotidase
EPS1	enhancer	−1		Protein disulfide isomerase-related protein involved in endoplasmic reticulum retention of resident ER proteins.
IDS2	enhancer	−2		Protein involved in modulation of Ime2p activity during meiosis
QDR3	suppressor	4		Multidrug transporter of the major facilitator superfamily, required for resistance to quinidine, barban, cisplatin, and bleomycin
TPO4	enhancer	−3		Polyamine transport protein, recognizes spermine, putrescine, and spermidine; localizes to the plasma membrane; member of the major facilitator superfamily
IZH3	enhancer	−2		Membrane protein involved in zinc metabolism, member of the four-protein IZH family, expression induced by zinc deficiency; deletion reduces sensitivity to elevated zinc and shortens lag phase, overexpression reduces Zap1p activity
		Unknown Function		
YKL063C	suppressor	4		Uncharacterized, GFP-fusion localizes to the Golgi
YML081W	suppressor	4	EGR3	Uncharacterized, GFP-fusion localizes to the nucleus
YNR014W	suppressor	4		Uncharacterized, expression is cell-cycle regulated and heat-inducible
YKL088W	suppressor	4	PPCDC	Protein required for cell viability. Predicted phosphopantothenoylcysteine decarboxylase
YML083C	suppressor	3		Uncharacterized, strong increase in transcript abundance during anaerobic growth compared to aerobic growth
YDR374C	suppressor	3	YTHDF1 YTHDF2 YTHDF3	Uncharacterized

Yeast Gene	Type	Strength	Human ortholog(s)	Proposed function
YOR291W (YPK9)	suppressor	3	ATP13A2 (PARK9) ATP13A3 ATP13A4 ATP13A5	Probable cation-transporting ATPase 2
YDL121C	suppressor	2		Uncharacterized, GFP-fusion localizes to the ER
YBR030W	suppressor	2		Uncharacterized, predicted to function in phospholipid metabolism
YMR111C	suppressor	2		Uncharacterized, GFP-fusion localizes to the nucleus
YOR129C	suppressor	2		Putative component of the outer plaque of the spindle pole body; may be involved in cation homeostasis or multidrug resistance.